ACS APPLIED MATERIALS & INTERFACES

www.acsami.org

Research Article

Scalable Electrically Conductive Spray Coating Based on Block Copolymer Nanocomposites

Junpyo Kwon, Katherine Evans, Le Ma, Daniel Arnold, M. Erden Yildizdag, Tarek Zohdi, Robert O. Ritchie, and Ting Xu*

Cite This: *ACS Appl. Mater. Interfaces* 2020, 12, 8687−8694

Read Online

ACCESS | Metrics & More | Article Recommendations | Supporting Information

ABSTRACT: Currently available conductive inks present a challenge to achieving electrical performance without compromising mechanical properties, scalability, and processability. Here, we have developed blends of carbon black and the commercially available triblock copolymer (BCP), poly(styrene-ethylene-butylene-styrene)-*g*-maleic anhydride (SEBS-*g*-MAH) (FG1924G, Kraton), that can be readily applied as a conductive coating via a spray-coating process, for a wide range of insulating materials (fabric, wood, glass, and plastic). Simple but effective mechanical and chemical modifications of the ingredients can increase the electrical conductivity (∼100 S/m) by an order of magnitude more than previously reported for carbon black composites; moreover, the coatings display excellent mechanical flexibility (tensile strain $\varepsilon \sim 5.00$ mm/mm). To correlate electrical conductivity and nanoscale structural changes with mechanical deformation, small-angle X-ray scattering (SAXS) during in situ tensile testing was performed. We show that the nanocomposite can be produced using low-cost ingredients (∼$ 10/kg), ensuring scalability for fabrication of large-scale devices without specialized material synthesis. Equally important, the phase behavior of block copolymers can enable recovery from physical damage via thermal annealing, which is critical for product longevity.

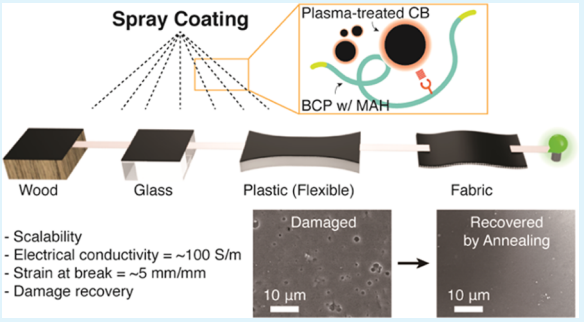

KEYWORDS: *conductive coatings, spray coatings, block copolymers nanocomposites, scalability, in situ small-angle X-ray scattering*

INTRODUCTION

The conductive ink market is projected to rapidly expand to a billion-dollar market[1] with the development of sensing,[2] internet of things (IoT), and machine-learning technologies.[3] Electric paint (E-paint) is one type of conductive ink that converts insulating surfaces into electrically conductive ones and additionally creates a human/electronic interface.[2−4] However, these materials are still in their infancy and cannot enable diverse interactive experiences because of their poor mechanical properties and low scalability. Therefore, new functional materials must be developed that simultaneously possess high mechanical flexibility, electrical conductivity, and critical scalability at low cost.[2,3]

Elastic and conductive nanocomposites (CNCs) have been extensively used for stretchable electronics,[5−7] strain gauges,[8,9] wearable devices,[4,10] actuators,[11] and filtering membranes.[12] Elastomers such as rubber, polyurethane, and poly(dimethylsiloxane) are commonly filled with conductive nanofillers such as gold nanoparticles,[13] silver nanowires,[14,15] or carbon-based materials to introduce electrical conductivity.[6,10,16−18] The conductivity can be increased by adding large amounts of fillers, but, at a certain point, material flexibility can be compromised.[19−22] Moreover, the conductivity exponentially decreases after stretching when disruptions to percolating networks of fillers occur.[18] Therefore, it is not sufficient to simply have a high-performance electrical and mechanical material. Design strategies for damage recovery are also required to prolong lifetime and durability.

In addition, CNCs are currently limited by the high cost of conductive fillers[22] (i.e., Ag flakes: ∼$ 1390/kg, Inframat). This becomes a critical bottleneck for device fabrication when scaling-up from millimeters to meters.[6,7,12] Carbon black is routinely used in CNCs because of its low cost and high conductivity.[23−26] In general, carbon black has a weak interaction with polymer chains and forms agglomerates that compromise the mechanical and electrical properties.[27] Such a deleterious effect is hard to overcome using the most commonly applied melt-mixing process because of high viscosity and limited input energy (i.e., processing time, temperature, and rotational mixing speed), which results in low electrical conductivity of the final CNC (0.1−20 S/m).[25,28−30]

Received: November 15, 2019
Accepted: January 23, 2020
Published: January 23, 2020

Here, we introduce a low cost (~$ 10/kg), yet mechanically flexible (tensile strain $\varepsilon \sim 5.00$ mm/mm), CNC (~100 S/m) material made from the commercially available elastomer, poly(styrene-ethylene-butylene-styrene) (SEBS) (Kraton), modified with maleic anhydride and carbon black, for spray-coating applications with no substrate limitation. The crucial, yet less studied, fundamental relationship between mechanical deformation and electrical conductivity is examined using small-angle X-ray scattering (SAXS) during in situ tensile testing coupled with conductivity measurements. Simple treatments of the ingredients can increase the conductivity more than ten times than the previously reported values as well as maintain conductivity over tens of S/m, when stretched ($\varepsilon \sim$ 1.60 mm/mm) until the formation of nanocavitation in the CNC. In addition, the damaged CNC coatings can be recovered by thermal annealing. The SEBS/carbon black blends enable electronics manufacturing at the meter-scale and at low cost, making them practical and highly attractive for device fabrication.

EXPERIMENTAL SECTION

Materials. Polystyrene-*co*-ethylene-*co*-butylene-*co*-styrene-*g*-maleic anhydride (SEBS-*g*-MAH) was provided by Kraton Polymers LLC (FG1924G); carbon black (Black Pearls 2000 Carbon Black) was purchased from Cabot. SEBS without MAH (cylindrical) and SEBS-*g*-MAH (cylindrical) were MD6971 and FG1901G, respectively (Kraton). The SEBS was dried at 50 °C in vacuo for an hour. The carbon black was ground and then oxidized under vacuum using a plasma cleaner for 10 min. The oxygen-treated carbon black was suspended in a 1:1 volume ratio of toluene/tetrahydrofuran and sonicated for an hour using a Fisher ultrasonication bath followed by probe-type sonication using a "1 s on 1 s off" cycle for 40 min. The mass ratio of the formula of the solution SEBS/carbon black/toluene-tetrahydrofuran = 1:0.5:9. Finally, the solvents were evaporated to the concentration of ~50 mg/mL using a rotary evaporator to achieve a desired viscosity for the spraying process. Thermal annealing was performed at 70 °C under vacuum for 12 h. The annealed samples were slowly cooled at room temperature.

Mechanical and Conductivity Testing. Uniaxial tensile tests were performed on a screw-driven mechanical testing machine (Instron-5933, Norwood, MA) with a 2 kN maximum load cell. The SEBS and carbon black solution was dried in a custom-designed Teflon mold at room temperature. All dried films (thickness of ~300 μm) were cut into dog-bone samples with an ASTM D1708 cutting die, with the exception of the sample ($f_{CB} = 0.27$) that was cut into a 5 × 30 mm^2 rectangular cross-section; specimen gauge lengths were set at 22 mm. Testing was carried out at room temperature at a cross-head speed of 10 mm/min for the tensile tests and 2 mm/min for the cyclic tests (to observe the Mullins effect[31]). More than five samples for each condition were tested. The cyclic tests were performed under load control in ambient air, using a servo-hydraulic MTS Tytron 250 mechanical testing machine (MTS Systems Corporation, Eden Prairie, MN). Loads were applied at frequencies of 5 and 10 Hz (sine wave). Electrical conductivity was measured using the automated four-point probe resistivity measurement system (Miller Design FPP-5000) and two-point probe methods with a commercial multimeter while stretching.

Characterization. X-ray photoelectron spectroscopy (XPS) measurements were performed with a PerkinElmer Phi 5600 using a monochromatic Al Kα X-ray source operated at 350 W. A charge neutralizer was used with an emission of 1 μA to inhibit charging of the samples. Transmission electron microscopy (TEM) imaging was performed on a FEI Tecnai 12 TEM at an accelerating voltage of 120 kV. Annealed samples were embedded in resin (Araldite 502, Electron Microscopy Sciences) and cured at 60 °C overnight. Thin sections, about 60 nm in thickness, were microtomed using an RMC MT-X ultramicrotome (Boeckler Instruments) and picked-up on copper TEM grids on top of water. For samples without the annealing process, cryo-microtoming was carried out. Scanning electron microscope (SEM) imaging was performed on a Hitachi S-5000. Atomic force microscope (AFM) imaging was conducted with a Bruker Dimension Edge AFM in the tapping mode using RTESPA-150 probes with a resonant frequency of ~150 kHz.

Tensile Testing and Drying with in Situ SAXS Measurements. Using the same preparation procedures as for the dog-bone-shaped tension samples, the specimens were loaded in tension while being simultaneously exposed to synchrotron X-rays at beamline 7.3.3 in the Advanced Light Source synchrotron radiation facility (Lawrence Berkeley National Laboratory, Berkeley, CA). The uniaxial tensile tests were performed in a Linkam TST-350 stage with a 45 N load cell (Omega, LC703-10) to measure the force. Such an experimental setup allows for SAXS data collection to be recorded in real time during the measurement of load−displacement curves. The mechanical tests were performed at room temperature at a displacement rate of 12 mm/min. The energy of the X-rays was 10 keV with a wavelength (λ_{wave}) of 0.127 nm. A Pilatus 2 M detector (Dectris Ltd., Baden, Switzerland) was used to collect two-dimensional (2D) scattering patterns with the resulting data calibrated using a Ag-behenate standard sample.

Adhesion Test. Peel tests (180°) were performed on a mechanical testing machine (Instron-5933) following ASTM Standard D903.[32]

RESULTS AND DISCUSSION

To prepare the flexible CNC (Figure 1a), a commercially available elastomer was blended with carbon black (~$ 0.1/kg).[33] Block copolymer (BCP) elastomers such as poly(styrene-ethylene-butylene-styrene) (SEBS) have high durability, thus making them an attractive CNC matrix. The microphase separation of BCP can be controlled via thermal[34] or solvent[35,36]

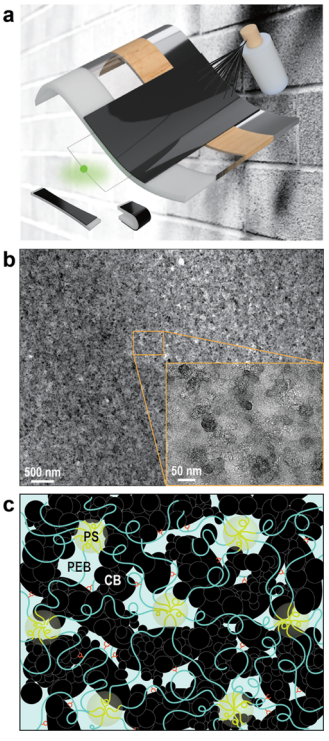

Figure 1. (a) Schematic drawing of the large-scale coating of designed SEBS/carbon black blends using a sprayer. (b) Transmission electron microscopy (TEM) images of the blends (volume fraction of the carbon black $f_{CB} \sim 0.20$). (c) The design of the blends as elastic conductive nanocomposites. The spherical region (green) represents the polystyrene region and the outer polymer matrix (blue) represents the poly(ethylene-butylene) region. Black particles represent the carbon black.

https://dx.doi.org/10.1021/acsami.9b20817
ACS Appl. Mater. Interfaces 2020, 12, 8687−8694

annealing or by an applied external field.[37,38] Upon microphase separation, the particles can be selectively incorporated into specific domains, which enables a controlled dispersion within the matrix.[19−21,34,36,39] However, proper mechanical and chemical treatments of carbon black are required to properly disperse the fillers. In addition, the effect of BCP morphology and composition on the physical properties can also play a role.

Carbon Black Treatments. Increasing the energy of mixing can break down the agglomerates of carbon black and induce good dispersions in a polymer matrix. Figure 2a shows that the conductivity can be increased if a higher energy of mixing is provided, such as with probe sonication as opposed to stirring. Favorable filler−elastomer interactions are needed to disperse the nanoparticles.[27] Plasma treatment of carbon black introduces hydrophilic oxygen-containing functional groups onto the filler surface such as hydroxyl groups.[40−43] X-ray photoelectron spectroscopy (XPS) results show high-intensity peaks at 285.0−289.1 eV, which correspond to the regions of aromatic hydroxyl, carbonyl, and carboxyl bonding[42,44] (Figure 2b). XPS confirmed that the overall ratios of carbon and oxygen on the surface of carbon black were 89.9 and 10.1%, respectively. Indeed, solvent mixing can help to achieve a higher conductivity than melt mixing.[25,28−30]

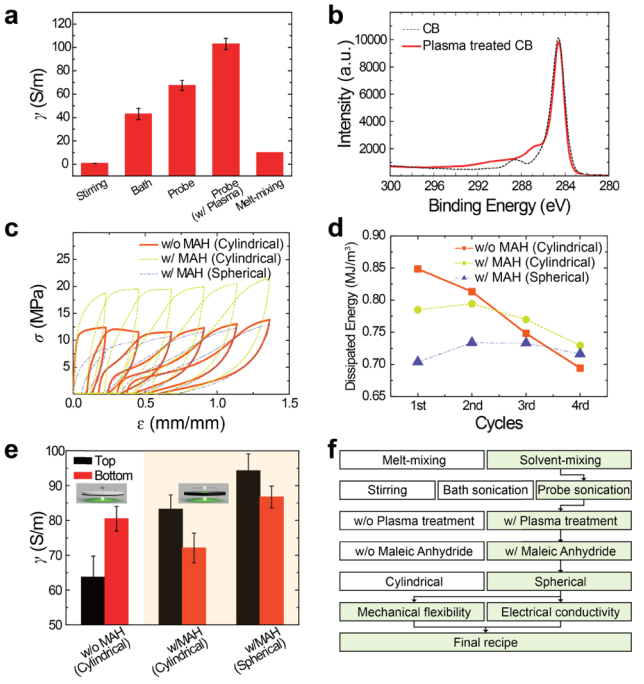

Figure 2. (a) Comparison of the electrical conductivities after different sample preparation methods ($f_{CB} \sim 0.20$). (b) XPS spectra of the plasma-untreated and -treated carbon black confirming surface modification. (c, d) Stress−strain curves under cyclic loading and the comparison of dissipated energies by different polymer matrices ($f_{CB} \sim 0.20$). (e) Comparison of electrical conductivities (top and bottom surfaces) for different polymer matrices. (f) Flow chart for the preparation of the blend.

Polymer Matrix Selection. The properties of the CNC depend on chemical modification of the BCP and on its morphology. In SEBS, the poly(ethylene-butylene) segment is functionalized with maleic anhydride (MAH) groups (1−1.7 wt %) that may form covalent bonds with the hydroxyl groups[45] on the modified carbon black; considering the dimensions of carbon black, the polymeric chains can favorably interact with other polar groups on its surface. Upon incorporation, the carbon black should act as a means of cross-linking to bridge the polymer chains in the BCP matrix, as schematically shown in Figure 1c. Three candidate composite compositions were tested with the following polymer matrices: polystyrene cylindrical morphology with and without MAH and spherical morphology with MAH.

Weak interactions between polymeric chains and fillers can induce chain/filler slip in elastomers, which results in cyclic stress softening;[46] this is known as the Mullins effect.[31] To verify the effect of MAH, the Mullins effect in SEBS/carbon black blends ($f_{CB} = 0.20$) was investigated (Figure 2c). During the first and second cycles, the cyclic stress-softening effect of SEBS without MAH was more dramatic than with the other two polymers with MAH. In addition, Figure 2d shows that the amount of dissipated energy in the SEBS-*g*-MAH was 10−15% lower than that of SEBS without MAH, which results from a higher interaction between the fillers and polymer chains.

Conductivity tests also show that MAH improves dispersions ($f_{CB} = 0.20$) of carbon black (Figure 2e). In the case of SEBS without MAH, the bottom surface has higher conductivity than the top. It means that carbon black aggregated at the bottom while the solvent evaporated. However, for SEBS-*g*-MAH, the overall conductivity increased, showing higher conductivity on the top than at the bottom.

The BCP morphology could be another important parameter because a percolation network[47] of carbon black must be formed to achieve electric conductivity. The BCP morphological effects on the conductivity were investigated using static SAXS. The SAXS results reveal that carbon black agglomerates with a spherical morphology of the polymer matrix are less interpenetrated than with a cylindrical morphology (Figure 3a). The slope of the intensity as a function of the scattering vector q observed in a log−log plot ($q < 0.1$ nm^{-1}) is determined by the mass fractal dimension (d_m);[48−53] the latter term is described in detail in Supporting Information, Note 1 and Figures S1 and S2. In the case of dilute dispersions of carbon black, the structure factor of the carbon black fractal aggregate dimension is close to −1.8.[48,49,51] The measured d_m values for the spherical and

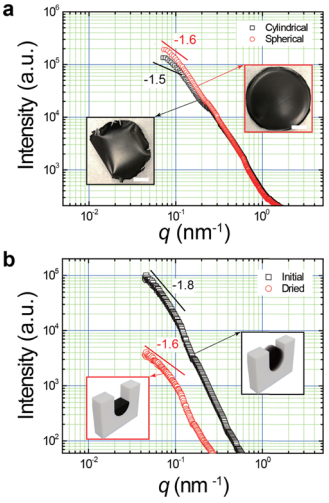

Figure 3. (a) Static SAXS results of cylindrical and spherical morphology of SEBS. The dry-cast films made of different polymer morphologies (scale bar: 50 mm); (b) SAXS intensity curves when spraying (initial) and drying.

https://dx.doi.org/10.1021/acsami.9b20817
ACS Appl. Mater. Interfaces 2020, 12, 8687−8694

cylindrical morphologies are −1.6 and −1.5, respectively. Thus, a spherical morphology helps to achieve better dispersions of carbon black, which results in higher conductivity than a cylindrical morphology.

Other advantages are evident when using SEBS-*g*-MAH, which forms a spherical morphology with polystyrene. The spherical morphology (13 wt % of polystyrene) is more flexible than the cylindrical morphology (30 wt %) because of a lower concentration of rigid polystyrene. Additionally, the spherical morphology develops upon solvent evaporation without further treatment, which is ideal for nonequilibrium, rapid CNC processes, such as spraying. As shown in the TEM image of the designed SEBS/carbon black blends (Figure 1b), the carbon black can be seen to be well dispersed within the SEBS matrix.

In situ SAXS was also used to monitor nanoscale structural changes during the CNC drying process that was performed during spray coating. Initially, the coating was in the liquid state with the value of d_m close to the ideal value ($d_m \sim -1.8$) for dilute dispersions of carbon black (Figure 3b). After the solution dried, d_m increased to −1.6. Considering that $d_m \sim -1.6$ of our sample is closer to −1.8 than the previously reported d_m value for carbon black composites (−0.7[49] to −1.3[50]), our in situ drying results verified that carbon black was well distributed within the SEBS matrix, not only in the liquid state but also in a dried state.

Relationship between Mechanical and Electrical Properties. The conductivity γ of SEBS/carbon black blends is shown in Figure 4a. As f_{CB} increases, the conductivity of the composite increases exponentially. At 20 vol % carbon black loading, the blends show a conductivity of ∼100 S/m. Further increases in the filler loading to 27 vol % leads to a conductivity of ∼315 S/m. This range of electrical conductivity can be applicable to many electronic devices such as printed circuit boards,[54] tracking sensing boards,[2,3] or electroencephalogram (EEG) monitoring systems.[4] The conductivity here was fitted using a well-known power-law theory for a percolating network.[47,54] The calculated values of the bulk conductivity of the carbon black (γ_0), the critical volume fraction at percolation (f_c), and the power-law exponent (s) were found to be 3.3×10^4 S/m, 0.11, and 2.48, respectively.

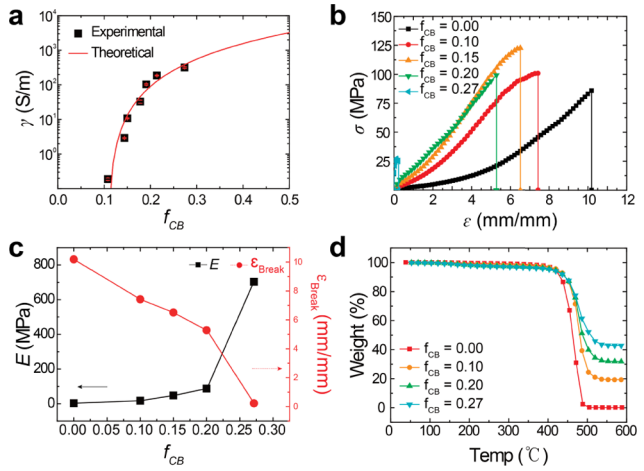

Figure 4. (a) Electrical conductivity γ changes as a function of f_{CB}. The solid line is the fitted curve based on experimental results with a percolating network theory. (b) Uniaxial tensile stress−strain curves of the blends. (c) Changes in Young's modulus E and fracture strain ε_{Break}. (d) Thermogravimetric analysis of the blends.

The mechanical properties of the SEBS/carbon black blends were measured by performing uniaxial tensile testing. The test samples were solvent-cast without further treatment to mimic the spray-coating process. The inclusion of the rigid carbon black markedly changed the mechanical behavior of the blends (Figure 4b). The measured values of Young's modulus (E) increased exponentially as f_{CB} increased from 0 to 0.27 (Figure 4c); the corresponding values of strain at break ε_{Break} decreased with increasing f_{CB}, as expected. For more in-depth studies, the SEBS/carbon black blend ($f_{CB} = 0.20$) was selected because the targeted CNC should possess appropriate flexibility and electrical conductivity.

In Situ SAXS with Tensile Testing. Since the conductivity of CNCs is governed by the number of conductive particles in contact, the electric conductivity varies with the deformation of the composites, thereby demonstrating piezoresistivity.[25] The critical challenge here is that the electrical conductivity exponentially decreases after the onset of plastic deformation, which can result in the original electrical properties being severely degraded.[18,54] However, little is known about the relationship between the nanoscale structural changes and electrical conductivity during the deformation of CNCs. Therefore, SAXS/conductivity measurements during in situ tensile testing were performed to study how nanoscale plastic deformation can affect the conductivity (Figure S3).

Figure 5a shows the SAXS/conductivity measurements taken in situ during the tensile tests. Initially, at a strain ε of zero, a radially symmetric two-dimensional scattering pattern appears, which means that the carbon black particles are randomly distributed in the polymer matrix. This is consistent with the proposed structure shown in Figure 1c. Stretching to the yield point (ε = 0.60) gradually induces a "butterfly-shaped" scattering pattern in the low q ($q < 0.1$ nm^{-1}) region. At this point, the electrical resistance barely increases. However, the butterfly-shaped pattern starts to deform at a strain of $\varepsilon \sim 1.50$ and evolves into a "lemon-shaped" pattern when stretched near the fracture point ($\varepsilon > 3.00$); at this transition, at a strain of ε = 1.66, the resistance starts to dramatically increase.

Schematic drawings in Figure 5b are shown to illustrate the nanoscale structural changes represented by each of the isotropic, butterfly-, and lemon-shaped SAXS patterns. The butterfly-shaped pattern at ε = 0.60 is attributed to the nonaffine deformation of the composite because the strong intensity along the stretch direction is due to the banded structures, lying at right angles to the tensile axis, that is formed by deformed carbon black aggregates separated by polymer chains.[48,49,55] With increased stretching of the sample, the transition from the butterfly- to the lemon-shaped pattern occurs concomitant with the appearance of nanocavitations, on the order of 90 × 105 nm in size;[48] further discussion of these nanocavitations is provided in Supporting Information Note 2 and Figure S4. The above two-dimensional pattern changes can also be qualitatively observed in Figure 5c with the intensity variations as a function of the azimuthal angle (Ψ). Figure 5d shows the change in the normalized scattering invariant Q/Q_0, which is a ratio of the integral of the intensity over all reciprocal space with Ψ in the low q range before and after deformation. At the lemon- to butterfly-shaped transition, Q/Q_0 increases exponentially as well, which indicates the onset of a disruption in the carbon black aggregate network.[48,49] Strikingly, the resistance starts to exponentially increase as well at this point. Hence, the in situ SAXS/conductivity measurements during tensile testing not only confirmed the existence of nanocavitations but also

https://dx.doi.org/10.1021/acsami.9b20817
ACS Appl. Mater. Interfaces 2020, 12, 8687−8694

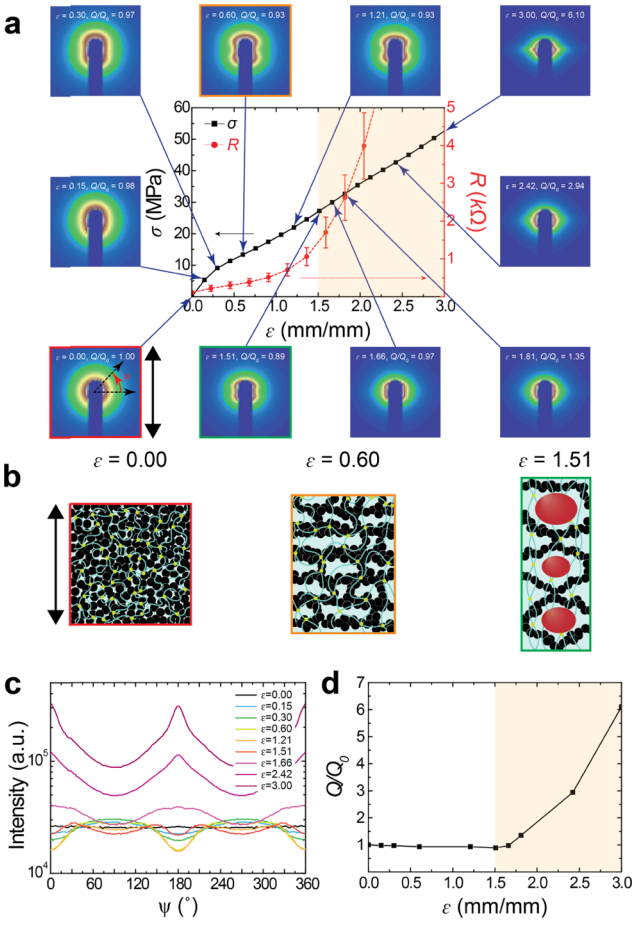

Figure 5. (a) Change in the stress−strain curve and electrical resistance of the SEBS/carbon black blends ($f_{CB} \sim 0.20$), with 2D SAXS patterns taken before and at the selected strains while stretching longitudinally along the axis of the specimen (a black arrow). (b) Schematic drawings of the nanoscale structural changes of SEBS/carbon black blends during uniaxial tensile stretching. The black arrow is the tensile direction and the red elliptical shapes are the nanocavitations. (c) Plots of the intensity as a function of the azimuthal angle (Ψ) in the low q ($q < 0.1$ nm^{-1}) region. (d) The change of the normalized scattering invariant (Q/Q_0) in the low q when stretching.

indicated that the nonaffine deformation of carbon black agglomerates (below a strain of $\varepsilon < 1.51$) barely contributes to the change in the conductivity. Accordingly, it is clear that our CNC can be bent and stretched while still maintaining good electrical conductivity.

Schematic drawings in Figure 5b are shown to illustrate the nanoscale structural changes represented by each of the isotropic, butterfly-, and lemon-shaped SAXS patterns. The butterfly-shaped pattern at $\varepsilon = 0.60$ is attributed to the nonaffine deformation of the composite because the strong intensity along the stretch direction is due to the banded structures, lying at right angles to the tensile axis, that is formed by deformed carbon black aggregates separated by polymer chains.[48,49,55] With increased stretching of the sample, the transition from the butterfly- to the lemon-shaped pattern occurs concomitant with the appearance of nanocavitations, on the order of 90 × 105 nm in size;[48] further discussion of these nanocavitations is provided in Supporting Information Note 2 and Figure S4. The above two-dimensional pattern changes can also be qualitatively observed in Figure 5c with the intensity variations as a function of the azimuthal angle (Ψ). Figure 5d shows the change in the normalized scattering invariant Q/Q_0, which is a ratio of the integral of the intensity over all reciprocal space with Ψ in the low q range before and after deformation. At the lemon- to butterfly-shaped transition, Q/Q_0 increases exponentially as well, which indicates the onset of a disruption in the carbon black aggregate network.[48,49] Strikingly, the resistance starts to exponentially increase as well at this point. Hence, the in situ SAXS/conductivity measurements during tensile testing not only confirmed the existence of nanocavitations but also indicated that the nonaffine deformation of carbon black agglomerates (below a strain of $\varepsilon < 1.51$) barely contributes to the change in the conductivity. Accordingly, it is clear that our CNC can be bent and stretched while still maintaining good electrical conductivity.

Spray-Coating Applications. The conductive SEBS/carbon black blends can be sprayed with a commercial spray to form uniform films on a range of substrates (shown in Supporting Information Movie 1). Figure 6a shows the SEBS/carbon black blend-coated substrates (three-dimensional (3D)-printed polymers, woods, metal, glass, and fabrics) connected in series. These results confirmed that a high electrical conductivity can be readily attained, sufficient to light a light-emitting diode (LED) with a 5 V power supply with a 5 kΩ resistance.

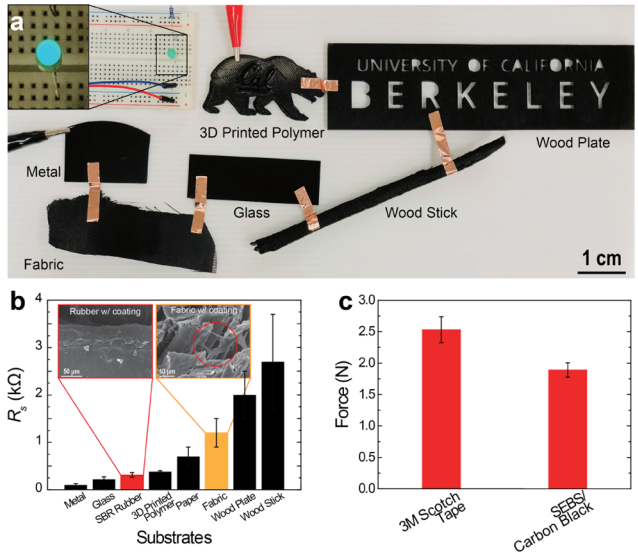

Figure 6. (a) Electric circuit made with different coated substrates: plastic, wood, metal, glass, and fabric. (b) Comparison of the electrical sheet resistance (R_s) of differing substrates when coated with the SEBS/carbon black blends. Inner SEM images show the coating status of rubber and fabric. (c) Comparison of adhesion forces with a 3 M Scotch tape.

For porous substrates like fabric and paper, the SEBS/carbon black blends can seep through the pores to provide electrical conductivity via large conducting interfaces. Scanning electron microscopy (SEM) images revealed that the pores in the fabric, which are typically sized in the tens of micrometers, are electrically bridged by the blends (Figure 6b). The coatings can span the pores and are flexible enough to maintain conductivity at high frequencies (10 Hz) despite the rapid vibration and deformation. In an adhesion test, the coating also exhibited a reasonable adhesion force (~1.9 N) on a metal plate, some 30% lower than that of the commercial 3 M Scotch tape (Figure 6c).

Damage Recovery via Thermal Annealing. All measurements up to this point were made on as-sprayed films with no

https://dx.doi.org/10.1021/acsami.9b20817
ACS Appl. Mater. Interfaces 2020, 12, 8687−8694

further treatment. Initially, it was shown that the films have good elastomeric and conductive properties. However, after repeated stretching or use at strains above the yield strain, these films will degrade; consequently, to be incorporated into long-lasting functional materials, the properties must be recoverable. Thermal annealing gives polymer chain mobility and thereby provides a means for the films to restore their original structure and electrical conductivity. We performed mechanical and conductivity analysis of the annealed SEBS/carbon black blends and compared the results with those from nominally identical samples that had not been annealed. It was observed that the mechanical strength and electrical conductivity were both higher in thermally annealed samples (Figure 7a,b). Interestingly, heat

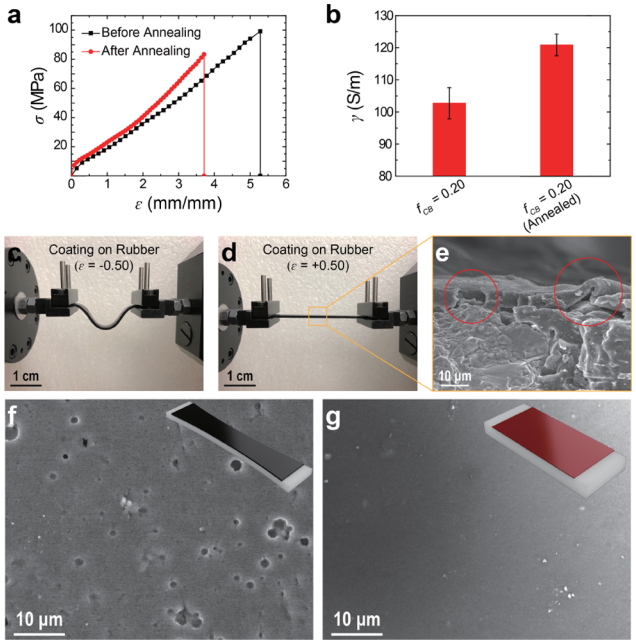

Figure 7. (a, b) Mechanical stress−strain curves and electrical conductivity measurements of the annealed vs unannealed SEBS/carbon black blends. (c, d) Cyclic tests on the SEBS/carbon black blend-coated SBR. (e) Cross-sectional SEM image showing physical damage resulting from plastic deformation of the coating (f, g). Top surface SEM images of the CNC-coated rubbers when damaged and after recovery.

treatment at temperatures below the glass-transition temperature of polystyrene ($T < T_{g,polystyrene}$) can be simply applied using a commercial heat gun (shown in Supporting Information Movie 2); following such treatments, the conductivity was found to recover, specifically, by increasing 20% in a mere half minute.

Thermal annealing also recovers any damage to the CNC and resultant disruption of the percolating networks of the carbon black. After stretching a coated substrate (SBR) a thousand times at a frequency (5 Hz) with a strain, $\varepsilon \sim \pm 0.50$ (Figure 7c,d), the samples were clearly damaged based on the SEM images (Figure 7e,f); in particular, the electrical conductivity was reduced by 20% from its initial value (Figure 8c). After annealing, however, the structure regained electrical conductivity and the porosity was eliminated (Figure 7g).

As BCPs order upon thermal annealing, we reasoned that both the BCP and incorporated carbon black can be rearranged during the annealing process. Figure 8a,b shows the TEM images of the SEBS/carbon black blends before and after thermal annealing. To see this thermal annealing effect, the

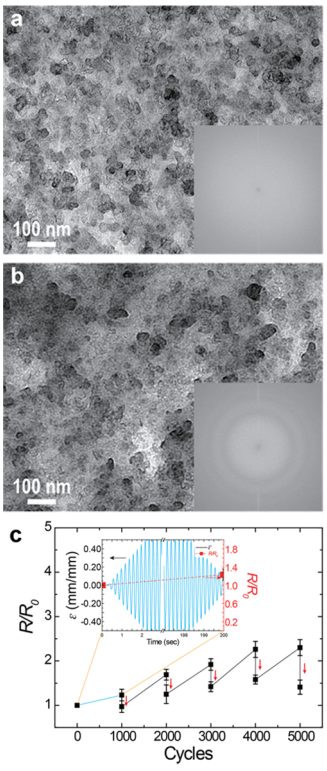

Figure 8. (a, b) TEM images of unannealed and annealed states of the SEBS/carbon black blends. Inset: the Fourier transform (FFT) image. (c) The conductivity changes in the SEBS/carbon black blends during 5000 stretching cycles at 5 Hz, followed by thermal annealing (red arrows). Inset: graph shows the first cyclic test.

coated substrates were again stretched, and then thermally annealed at 70 °C. Figure 8c shows that the conductivity rarely changed even after stretching 5000 times; indeed, the recovery of the electrical conductivity can be achieved continuously in four additional loading and annealing cycles.

CONCLUSIONS

We have presented in this study a composite based on a commercially available and functionalized block copolymer elastomer and carbon black for elastic conductive coating applications. BCP-guided dispersions of nanoparticles were achieved using plasma-treated carbon black, which results in electrical conductivity ten times higher than the previously reported values for carbon black composites and with a ductility (or breaking strain) of over 5 mm/mm. The structure of the nanocomposite was monitored while simultaneously measuring conductivity to provide insight into the structure/conductivity relationship. This functional CNC can easily be sprayed onto diverse substrates. Moreover, if its mechanical and electrical properties degrade after multiple use, they can be continuously recovered by thermal annealing due to reordering of the BCP matrix. Accordingly, we believe that the manufacturing of large-scale elastic conductive coatings is definitively feasible with this low-cost, recoverable BCP-based nanocomposite.

ASSOCIATED CONTENT

Supporting Information

The Supporting Information is available free of charge at https://pubs.acs.org/doi/10.1021/acsami.9b20817.

https://dx.doi.org/10.1021/acsami.9b20817
ACS Appl. Mater. Interfaces 2020, 12, 8687−8694

Mass fractal dimension, d_m; size of the nano-caviations; schematic drawings of carbon black object, cluster, and the elliptically deformed cluster; experimental set-up for the synchrotron SAXS (PDF)

Video_S1. Small angle X-ray scattering results (MP4)

Video_S2. Heat treatment at temperatures below the glass-transition temperature of polystyrene (MP4)

AUTHOR INFORMATION

Corresponding Author

Ting Xu − *Materials Sciences Division, Lawrence Berkeley National Laboratory, Berkeley, California 94720, United States; Department of Chemistry and Department of Materials Science and Engineering, University of California, Berkeley, California 94720, United States;* orcid.org/0000-0002-2831-2095; Email: tingxu@berkeley.edu

Authors

Junpyo Kwon − *Department of Mechanical Engineering, University of California, Berkeley, California 94720, United States; Materials Sciences Division, Lawrence Berkeley National Laboratory, Berkeley, California 94720, United States*

Katherine Evans − *Materials Sciences Division, Lawrence Berkeley National Laboratory, Berkeley, California 94720, United States; Department of Chemistry, University of California, Berkeley, California 94720, United States*

Le Ma − *Materials Sciences Division, Lawrence Berkeley National Laboratory, Berkeley, California 94720, United States; Department of Materials Science and Engineering, University of California, Berkeley, California 94720, United States*

Daniel Arnold − *Department of Chemical Engineering, University of California, Berkeley, California 94720, United States*

M. Erden Yildizdag − *Department of Mechanical Engineering, University of California, Berkeley, California 94720, United States*

Tarek Zohdi − *Department of Mechanical Engineering, University of California, Berkeley, California 94720, United States*

Robert O. Ritchie − *Department of Mechanical Engineering and Department of Materials Science and Engineering, University of California, Berkeley, California 94720, United States; Materials Sciences Division, Lawrence Berkeley National Laboratory, Berkeley, California 94720, United States;* orcid.org/0000-0002-0501-6998

Complete contact information is available at: https://pubs.acs.org/10.1021/acsami.9b20817

Notes

The authors declare no competing financial interest.

ACKNOWLEDGMENTS

This work was funded by the U.S. Department of Energy, Office of Science, Office of Basic Energy Sciences, Materials Sciences and Engineering Division under Contract DE-AC02-05-CH11231 (Organic−Inorganic Nanocomposites KC3104). SAXS was performed at beamline 7.3.3 at the Advanced Light Source, which is supported by the U.S. Department of Energy, Office of Science, Office of Basic Energy Sciences, under contract no. DE-AC02-05-CH11231. J.K. was supported at UC Berkeley by a Jane Lewis Fellowship.

REFERENCES

(1) Xie, R.; Xie, Y.; López-Barrón, C. R.; Gao, K.-Z.; Wagner, N. J. Ultra-Stretchable Conductive Iono-Elastomer and Motion Strain Sensor System Developed Therefrom. *Technol. Innovation* **2018**, *19*, 613−626.

(2) Zhang, Y.; Laput, G.; Harrison, C. In *Electrick: Low-Cost Touch Sensing Using Electric Field Tomography*, Proceedings 2017 CHI Conference on Human Factors in Computing Systems; ACM, 2017; pp 1−14.

(3) Zhang, Y.; Yang, C.; Hudson, S. E.; Harrison, C. In *Sample, A. In Wall ++: Room-Scale Interactive and Context-Aware Sensing*, Proceedings 2018 CHI Conference on Human Factors inComputing Systems; ACM, 2018; pp 1−15.

(4) Joong Hoon, L.; Seung Min, L.; Hang Jin, B.; Joung Sook, H.; Kwang Suk, P.; Sang-Hoon, L. Cnt/Pdms-Based Canal-Typed Ear Electrodes for Inconspicuous Eeg Recording. *J. Neural Eng.* **2014**, *11*, No. 046014.

(5) Catenacci, M. J.; Reyes, C.; Cruz, M. A.; Wiley, B. J. Stretchable Conductive Composites from Cu−Ag Nanowire Felt. *ACS Nano* **2018**, *12*, 3689−3698.

(6) Sekitani, T.; Noguchi, Y.; Hata, K.; Fukushima, T.; Aida, T.; Someya, T. A Rubberlike Stretchable Active Matrix Using Elastic Conductors. *Science* **2008**, *321*, 1468−1472.

(7) Wang, Y.; Zhu, C.; Pfattner, R.; Yan, H.; Jin, L.; Chen, S.; Molina-Lopez, F.; Lissel, F.; Liu, J.; Rabiah, N. I.; et al. A Highly Stretchable, Transparent, and Conductive Polymer. *Sci. Adv.* **2017**, *3*, No. e1602076.

(8) Park, M.; Im, J.; Shin, M.; Min, Y.; Park, J.; Cho, H.; Park, S.; Shim, M.-B.; Jeon, S.; Chung, D.-Y.; et al. Highly Stretchable Electric Circuits from a Composite Material of Silver Nanoparticles and Elastomeric Fibres. *Nat. Nanotechnol.* **2012**, *7*, 803−809.

(9) Li, X.; Zhang, R.; Yu, W.; Wang, K.; Wei, J.; Wu, D.; Cao, A.; Li, Z.; Cheng, Y.; Zheng, Q. Stretchable and Highly Sensitive Graphene-on-Polymer Strain Sensors. *Sci. Rep.* **2012**, *2*, No. 870.

(10) Lipomi, D. J.; Vosgueritchian, M.; Tee, B. C.; Hellstrom, S. L.; Lee, J. A.; Fox, C. H.; Bao, Z. Skin-Like Pressure and Strain Sensors Based on Transparent Elastic Films of Carbon Nanotubes. *Nat. Nanotechnol.* **2011**, *6*, 788−792.

(11) Park, K. I.; Lee, M.; Liu, Y.; Moon, S.; Hwang, G. T.; Zhu, G.; Kim, J. E.; Kim, S. O.; Kim, D. K.; Wang, Z. L.; Lee, K. J. Flexible Nanocomposite Generator Made of Batio3 Nanoparticles and Graphitic Carbons. *Adv. Mater.* **2012**, *24*, 2999−3004.

(12) Jeong, S.; Cho, H.; Han, S.; Won, P.; Lee, H.; Hong, S.; Yeo, J.; Kwon, J.; Ko, S. H. High Efficiency, Transparent, Reusable, and Active Pm2. 5 Filters by Hierarchical Ag Nanowire Percolation Network. *Nano Lett.* **2017**, *17*, 4339−4346.

(13) Kim, Y.; Zhu, J.; Yeom, B.; Di Prima, M.; Su, X.; Kim, J.-G.; Yoo, S. J.; Uher, C.; Kotov, N. A. Stretchable Nanoparticle Conductors with Self-Organized Conductive Pathways. *Nature* **2013**, *500*, 59.

(14) Xu, F.; Zhu, Y. Highly Conductive and Stretchable Silver Nanowire Conductors. *Adv. Mater.* **2012**, *24*, 5117−5122.

(15) Lee, P.; Ham, J.; Lee, J.; Hong, S.; Han, S.; Suh, Y. D.; Lee, S. E.; Yeo, J.; Lee, S. S.; Lee, D.; Ko, S. H. Highly Stretchable or Transparent Conductor Fabrication by a Hierarchical Multiscale Hybrid Nanocomposite. *Adv. Funct. Mater.* **2014**, *24*, 5671−5678.

(16) Chiou, K.; Byun, S.; Kim, J.; Huang, J. Additive-Free Carbon Nanotube Dispersions, Pastes, Gels, and Doughs in Cresols. *Proc. Natl. Acad. Sci. U.S. A.* **2018**, *115*, 5703−5708.

(17) Liu, T.; Kou, T.; Bulmahn, D.; Ortuno-Quintana, C.; Liu, G.; Lu, J. Q.; Li, Y. Tuning the Electrochemical Properties of Nitrogen-Doped Carbon Aerogels in a Blend of Ammonia and Nitrogen Gases. *ACS Appl. Energy Mater.* **2018**, *1*, 5043−5053.

(18) Mates, J. E.; Bayer, I. S.; Palumbo, J. M.; Carroll, P. J.; Megaridis, C. M. Extremely Stretchable and Conductive Water-Repellent Coatings for Low-Cost Ultra-Flexible Electronics. *Nat. Commun.* **2015**, *6*, No. 8874.

(19) Warren, S. C.; Messina, L. C.; Slaughter, L. S.; Kamperman, M.; Zhou, Q.; Gruner, S. M.; DiSalvo, F. J.; Wiesner, U. Ordered

Mesoporous Materials from Metal Nanoparticle−Block Copolymer Self-Assembly. *Science* **2008**, *320*, 1748.
(20) Bockstaller, M. R.; Mickiewicz, R. A.; Thomas, E. L. Block Copolymer Nanocomposites: Perspectives for Tailored Functional Materials. *Adv. Mater.* **2005**, *17*, 1331−1349.
(21) Balazs, A. C.; Emrick, T.; Russell, T. P. Nanoparticle Polymer Composites: Where Two Small Worlds Meet. *Science* **2006**, *314*, 1107.
(22) Noh, J.-S. Conductive Elastomers for Stretchable Electronics, Sensors and Energy Harvesters. *Polymers* **2016**, *8*, 123.
(23) Luo, J.; Tung, V. C.; Koltonow, A. R.; Jang, H. D.; Huang, J. Graphene Oxide Based Conductive Glue as a Binder for Ultracapacitor Electrodes. *J. Mater. Chem.* **2012**, *22*, 12993−12996.
(24) Phillips, C.; Al-Ahmadi, A.; Potts, S.-J.; Claypole, T.; Deganello, D. The Effect of Graphite and Carbon Black Ratios on Conductive Ink Performance. *J. Mater. Sci.* **2017**, *52*, 9520−9530.
(25) Horibe, H.; Kamimura, T.; Yoshida, K. Electrical Conductivity of Polymer Composites Filled with Carbon Black. *Jpn. J. Appl. Phys.* **2005**, *44*, 2025.
(26) Leigh, S. J.; Bradley, R. J.; Purssell, C. P.; Billson, D. R.; Hutchins, D. A. A Simple, Low-Cost Conductive Composite Material for 3d Printing of Electronic Sensors. *PloS One* **2012**, *7*, No. e49365.
(27) Donnet, J.; Vidal, A. Carbon Black: Surface Properties and Interactions with Elastomers. *Adv. Polym. Sci.* **1986**, *76*, 103−127.
(28) Kuester, S.; Merlini, C.; Barra, G. M. O.; Ferreira, J. C.; Lucas, A.; de Souza, A. C.; Soares, B. G. Processing and Characterization of Conductive Composites Based on Poly(Styrene-B-Ethylene-Ran-Butylene-B-Styrene) (Sebs) and Carbon Additives: A Comparative Study of Expanded Graphite and Carbon Black. *Composites, Part B* **2016**, *84*, 236−247.
(29) Zucolotto, V.; Avlyanov, J.; Mattoso, L. H. C. Elastomeric Conductive Composites Based on Conducting Polymer−Modified Carbon Black. *Polym. Compos.* **2004**, *25*, 617−621.
(30) Pavlovsky, S.; Siegmann, A. Chemical Sensing Materials. I. Electrically Conductive Sebs Copolymer Systems. *J. Appl. Polym. Sci.* **2009**, *113*, 3322−3329.
(31) Mullins, L. Softening of Rubber by Deformation. *Rubber Chem. Technol.* **1969**, *42*, 339−362.
(32) Astm D903-98 *Standard Test Method for Peel or Stripping Strength of Adhesive Bonds*; ASTM Interntational, 2017.
(33) Roy, C.; Labrecque, B.; de Caumia, B. Recycling of Scrap Tires to Oil and Carbon Black by Vacuum Pyrolysis. *Resour., Conserv. Recycl.* **1990**, *4*, 203−213.
(34) Zhao, Y.; Thorkelsson, K.; Mastroianni, A. J.; Schilling, T.; Luther, J. M.; Rancatore, B. J.; Matsunaga, K.; Jinnai, H.; Wu, Y.; Poulsen, D.; et al. Small-Molecule-Directed Nanoparticle Assembly Towards Stimuli-Responsive Nanocomposites. *Nat. Mater.* **2009**, *8*, 979.
(35) Zhou, Z.; Liu, G. Controlling the Pore Size of Mesoporous Carbon Thin Films through Thermal and Solvent Annealing. *Small* **2017**, *13*, No. 1603107.
(36) Kao, J.; Thorkelsson, K.; Bai, P.; Zhang, Z.; Sun, C.; Xu, T. Rapid Fabrication of Hierarchically Structured Supramolecular Nanocomposite Thin Films in One Minute. *Nat. Commun.* **2014**, *5*, No. 4053.
(37) Majewski, P. W.; Gopinadhan, M.; Osuji, C. O. Magnetic Field Alignment of Block Copolymers and Polymer Nanocomposites: Scalable Microstructure Control in Functional Soft Materials. *J. Polym. Sci., Part B: Polym. Phys.* **2012**, *50*, 2−8.
(38) Hoheisel, T. N.; Hur, K.; Wiesner, U. B. Block Copolymer-Nanoparticle Hybrid Self-Assembly. *Prog. Polym. Sci.* **2015**, *40*, 3−32.
(39) Nedelcu, M.; Lee, J.; Crossland, E. J. W.; Warren, S. C.; Orilall, M. C.; Guldin, S.; Hüttner, S.; Ducati, C.; Eder, D.; Wiesner, U.; Steiner, U.; Snaith, H. J. Block Copolymer Directed Synthesis of Mesoporous Tio2 for Dye-Sensitized Solar Cells. *Soft Matter* **2009**, *5*, 134−139.
(40) Takada, T.; Nakahara, M.; Kumagai, H.; Sanada, Y. Surface Modification and Characterization of Carbon Black with Oxygen Plasma. *Carbon* **1996**, *34*, 1087−1091.
(41) De Torre, L. C.; Bottani, E.; Martinez-Alonso, A.; Cuesta, A.; Garcia, A.; Tascon, J. Effects of Oxygen Plasma Treatment on the Surface of Graphitized Carbon Black. *Carbon* **1998**, *36*, 277−282.
(42) Li, X.; Horita, K. Electrochemical Characterization of Carbon Black Subjected to Rf Oxygen Plasma. *Carbon* **2000**, *38*, 133−138.
(43) Park, S.-J.; Cho, K.-S.; Ryu, S.-K. Filler−Elastomer Interactions: Influence of Oxygen Plasma Treatment on Surface and Mechanical Properties of Carbon Black/Rubber Composites. *Carbon* **2003**, *41*, 1437−1442.
(44) Asai, S.; Kaneki, H.; Sumita, M.; Miyasaka, K. Effect of Oxidized Carbon Black on the Mechanical Properties and Molecular Motions of Natural Rubber Studied by Pulse Nmr. *J. Appl. Polym. Sci.* **1991**, *43*, 1253−1257.
(45) Evtushenko, Y. M.; Zaitsev, B. E.; Ivanov, V. M. Maleic Anhydride as a Reagent for the Determination of Hydroxyl Groups in Organic Compounds. *J. Anal. Chem.* **2000**, *55*, 859−862.
(46) Cantournet, S.; Desmorat, R.; Besson, J. Mullins Effect and Cyclic Stress Softening of Filled Elastomers by Internal Sliding and Friction Thermodynamics Model. *Int. J. Solids Struct.* **2009**, *46*, 2255−2264.
(47) Stauffer, D.; Aharony, A. *Introduction to Percolation Theory*, CRC Press, 1994.
(48) Zhang, H.; Scholz, A. K.; de Crevoisier, J.; Vion-Loisel, F.; Besnard, G.; Hexemer, A.; Brown, H. R.; Kramer, E. J.; Creton, C. Nanocavitation in Carbon Black Filled Styrene−Butadiene Rubber under Tension Detected by Real Time Small Angle X-Ray Scattering. *Macromolecules* **2012**, *45*, 1529−1543.
(49) Ehrburger-Dolle, F.; Bley, F.; Geissler, E.; Livet, F.; Morfin, I.; Rochas, C. Filler Networks in Elastomers. *Macromol. Symp.* **2003**, *200*, 157−168.
(50) Ehrburger-Dolle, F.; Hindermann-Bischoff, M.; Livet, F.; Bley, F.; Rochas, C.; Geissler, E. Anisotropic Ultra-Small-Angle X-Ray Scattering in Carbon Black Filled Polymers. *Langmuir* **2001**, *17*, 329−334.
(51) Schneider, G. J.; Göritz, D. Strain Induced Anisotropies in Silica Polydimethylsiloxane Composites. *J. Chem. Phys.* **2010**, *133*, No. 024903.
(52) Schneider, G. J. Correlation of Mass Fractal Dimension and Asymmetry. *J. Chem. Phys.* **2009**, *130*, No. 234912.
(53) Sorensen, C. M.; Oh, C.; Schmidt, P. W.; Rieker, T. P. Scaling Description of the Structure Factor of Fractal Soot Composites. *Phys. Rev. E* **1998**, *58*, 4666−4672.
(54) Valentine, A. D.; Busbee, T. A.; Boley, J. W.; Raney, J. R.; Chortos, A.; Kotikian, A.; Berrigan, J. D.; Durstock, M. F.; Lewis, J. A. Hybrid 3d Printing of Soft Electronics. *Adv. Mater.* **2017**, *29*, No. 1703817.
(55) Witten, T.; Rubinstein, M.; Colby, R. Reinforcement of Rubber by Fractal Aggregates. *J. Phys. II* **1993**, *3*, 367−383.

https://dx.doi.org/10.1021/acsami.9b20817
ACS Appl. Mater. Interfaces 2020, 12, 8687−8694